

Essential Features: Content-Adaptive Pixel Discretization to Improve Model Robustness to Adaptive Adversarial Attacks

Ryan Feng¹, Wu-chi Feng², Atul Prakash¹

¹University of Michigan, ²Portland State University

¹{rtfeng, aprakash}@umich.edu, ²{wuchi}@pdx.edu

Abstract

Preprocessing defenses such as pixel discretization are appealing to remove adversarial attacks due to their simplicity. However, they have been shown to be ineffective except on simple datasets such as MNIST. We hypothesize that existing discretization approaches failed because using a fixed codebook for the entire dataset limits their ability to balance image representation and codeword separability. We propose a per-image adaptive preprocessing defense called *Essential Features*, which first applies adaptive blurring to push perturbed pixel values back to their original value and then discretizes the image to an image-adaptive codebook to reduce the color space. *Essential Features* thus *constrains the attack space* by forcing the adversary to perturb large regions both locally and color-wise for its effects to survive the preprocessing. Against adaptive attacks, we find that our approach increases the L_2 and L_∞ robustness on higher resolution datasets.

1 Introduction

Machine learning models have been used for a large diversity of tasks including robots, speech recognition systems, and self-driving cars. These models, however, have been shown to be vulnerable to subtle adversarial attacks [1, 2, 3, 4, 5, 6], threatening the safety and real-world practicality of such systems.

Image preprocessing techniques such as JPEG compression [7, 8, 9], color-bit reduction [9, 10], and blurring [10] were proposed as early approaches towards defending image classification models against adversarial attacks. Such techniques were appealing because they were computationally cheap and simply applied, with the intuition being they could reduce adversarial effects without drastically changing the appearance of the image. These defenses, however, were later defeated with adaptive attacks that accounted for the transform [11].

Chen et al. [12] argue that pixel discretization approaches are unlikely to ever provide robustness on all but the simplest datasets. To back this claim, they extract theoretical and empirical insights on an approach that reduces the color space to dataset specific codebooks (a set of allowed codeword colors). They found that their technique succeeded on simple datasets like MNIST but failed on more practical datasets due to a lack of globally-separated color clusters.

We observe that such discretization techniques must inherently trade-off *representation*, the ability to preserve the essential features of the natural image required for classification, and *separability*, the scale of the space between codeword colors. Particularly with more complex datasets such as CIFAR-10 [13], where more colors are present in the natural data, codebooks with fewer colors tend to not have enough colors to represent the natural images well enough while codebooks with more colors will have less separation between the codewords.



Figure 1: *Essential Features* applies adaptive blurring and color reduction to constrain the attack space to a smaller color space. Left of each pair: attacked image. Right of each pair: transformed versions of the attacked image.

Our key insight is that we can improve the representation-separability trade-off with an *adaptive* transformation tailored to the content of each image. This is because individual images can have good color separability while the overall dataset has poor separability (i.e., there does not exist a single codebook that suffices for all images). For instance, a STOP traffic sign is predominantly red and white and has good separability. Similarly, an image of a flamingo against a water background may have good separability, but may require the inclusion of pink, which could be close to red if using a single codebook for both.

Essential Features consists of two-phases designed to constrain the attack space. First, *Essential Features* applies edge-aware adaptive blurring, which leverages spatial correlation to bias perturbed pixels back towards their original value while still preserving the essential edge features required for classification. This forces the adversary to perturb larger local regions in the same way to survive the blurring. Second, we apply a variant of k -means color reduction to reduce the adaptively blurred image into k separable color codeword colors, where k is chosen adaptively and tailored to each image. This forces the adversary to move pixels assigned to the same codeword color in the same direction to change the codeword’s location (although there will also be a limited number of pixels on the boundaries that can be reassigned to different codewords).

We empirically find that applying our *Essential Features* transformation with adversarial training generally increases the L_2 robustness compared against adversarial training baselines (e.g., 20.15% to 38.46% for CIFAR-10 [13] and 12.09% to 52.44% for RESISC45 [14]). We also find that on datasets with simpler colors such as MNIST and Fashion MNIST prior discretization work [12] also increases the L_2 robustness, with *Essential Features* typically providing better performance on more complex datasets. *Essential Features* also increases the L_∞ robustness on higher resolution datasets, where more aggressive feature reduction can occur without loss of detail (e.g., 43.89% to 53.33% on RESISC45 and 75.97% to 80.71% on Imagenette [15]).

Our contributions are as follows:

1. We demonstrate the utility of an adaptive, per-image discretization defense with a proof-of-concept example showing that adaptive strategies can increase robustness. (Section 3)
2. We propose a novel, content-aware defense called *Essential Features* that applies adaptive blurring and adaptive color discretization, which better balances the representation-separability trade-off. (Section 4)
3. We show that *Essential Features* increases the attack cost by raising the L_2 robustness (e.g., increase of 18.31% for CIFAR-10, 40.35% for RESISC45). We also raise the L_∞ robustness on higher resolution datasets (e.g., increase of 9.44% for RESISC45, 4.74% for Imagenette). (Section 5)

2 Related Work

2.0.1 Image Preprocessing Defenses

Image preprocessing approaches seek to remove adversarial perturbations through image processing (e.g., image blurring or sharpening) before handing the image to the machine learning model. The goal of such image preprocessing techniques is to both not affect the accuracy in classifying non-adversarial images as well as improving the classification accuracy of adversarially tampered images.

Several preprocessing defenses include color-bit reduction [9, 10], JPEG compression [7, 8, 9], and a non-differentiable pixel deflection approach [16]. These image preprocessing algorithm defenses were broken with simple applications of BPDA with the identity function as the backwards approximation [17, 11]. Xu et al. additionally propose filtering defenses but do not present adaptive attacks. Unlike our adaptive blurring, their filters are fixed. Liang et al. propose a per image adaptive detection approach that blurs each image based on its entropy [18]. In contrast, we propose a defense that outputs correct predictions in the face of attacks and blurs adaptively within an image.

More recently, Chen et al. propose a dataset tuned color codebook discretization algorithm that reduces each image to the same set of separable codebook colors [12]. They also suggest theoretically that such techniques are fundamentally doomed on complex datasets such as CIFAR-10 or ImageNet due to a lack of color separation in the dataset. We find that applying *Essential Features* on a *per-image basis* can constrain the attack space on additional datasets.

Jalalpour et al. [19] first proposed the notion of using k -means color reduction to thwart adversarial attacks. We also use a variant of k -means color reduction; however, unlike Jalalpour et al., we choose the number of colors k adaptively per image such that the chosen clusters are highly separable. Further, Jalalpour et al. did not adversarially train networks with k -means color reduced images. We additionally add adaptive Gaussian blurring before color reduction rather than normal Gaussian blurring, which preserves more of the original edge features.

2.0.2 Adversarial Training

Adversarial training is a common class of defense approaches that train classifiers under attacked images to raise robustness. The goal is that training on adversarial images will result in a hardened classifier. Adversarial training poses a min-max problem where we minimize the classifier’s loss over the strongest perturbations we can generate within the perturbation space [20]. Formally, it solves the following optimization problem:

$$\min_{\theta} \left(\mathbb{E}_{(x,y) \sim D} \left[\max_{\delta \in \mathcal{S}} L(\theta, x + \delta, y) \right] \right)$$

where x is an input image, y is the label, D is the data distribution, δ is the perturbation, \mathcal{S} is the allowable space of perturbations, L is the loss function, and θ are the model parameters.

One approach is Madry-style Adversarial training [20], which trains classifiers on Projected Gradient Descent (PGD) [20] attacks generated at each epoch. While effective, one limitation of adversarial training is that it is slow and hard to scale [21], so other approaches have tried to speed up adversarial training while retaining comparable accuracy [22, 23, 24, 25, 26]. We use ATTA [26], a technique that leverages cross-epoch transferability.

3 Motivation

We first motivate the viability of adaptive codebooks with a proof-of-concept example. We then discuss design considerations including the balance between *representation* and *separability*.

3.1 Proof-of-Concept

3.1.1 Preliminaries

Let $\mathcal{C}_F = \{c_1, c_2, \dots, c_n\}$ be a set of n colors. Let $FC(x, \mathcal{C}_F)$ be a fixed function that discretizes each pixel $x[i, j]$ within the image size with the value of the nearest color $c_i \in \mathcal{C}_F$. Let $AC(x)$ refer to any function that, extracts an adaptive codebook \mathcal{C}_A for x and then discretizes each pixel $x[i, j]$ with the value of the nearest color $c_i \in \mathcal{C}_A$. Let the range for each pixel $x_{i,j} \in x$ be $[0, 1]$.

Let our dataset be a generalized form of the MNIST dataset called MNIST_G , consisting of discretized images set to all possible pairs of colors w apart:

$$\text{MNIST}_D = \{FC(x, \{0, 1\}) : x \in \text{MNIST}\} \quad (1)$$

$$T = \{(x, c_1, c_2) \in \text{MNIST}_D \times \mathbb{R} \times \mathbb{R} : 0 \leq c_1 \leq 1, 0 \leq c_2 \leq 1, c_2 - c_1 \geq w\} \quad (2)$$

$$\text{MNIST}_G = \{FC(x, \{c_1, c_2\}) : (x, c_1, c_2) \in T\} \quad (3)$$

Finally, we define the *cluster assignment property* below, given an original input image x and a transformed image x' . The property states that for all pairs of pixels where their color matches in x , their colors will match also in x' .

$$\forall i_1 \forall j_1 \forall i_2 \forall j_2 \quad x[i_1, j_1] = x[i_2, j_2] \implies x'[i_1, j_1] = x'[i_2, j_2] \quad (4)$$

If the cluster assignment property is held, we know that there exists a well-performing model on MNIST_G , because prior work shows that discretizing MNIST images to 0 and 1 is robust [12]. The model would then just have to remap the output of the discretization function to 0 and 1 or learn to just use the comparative color difference between the two regions, leading to Theorem 1.

Theorem 1. *There exists an adaptive codebook function $AC(x)$ that maintains the Cluster Assignment Property under larger L_∞ perturbation bounds than all possible fixed codebook functions $FC(x, \mathcal{C}_F)$ on MNIST_G .*

Proof.

Lemma 1. *All fixed codebook functions $FC(x, \mathcal{C}_F)$ fail to maintain a robustness greater than a tiny ϵ .*

If there are two or more colors in \mathcal{C}_F , there must exist a midpoint between any arbitrary pair of adjacent codebook colors c_x and c_y . Let c_x refer to the smaller of the two colors and let $c_m = (c_x + c_y)/2$. Now, suppose we encounter an input example from MNIST_G that had used the following two colors for c_1 and c_2 : $c_1 = c_m$ and $c_2 = c_m + w$. Under an infinitesimally small perturbation bound $\epsilon > 0$, an adversary can violate the Cluster Assignment Property by adding ϵ to some pixels in c_1 to set it to c_y and subtracting ϵ to some pixels in c_1 to set it to c_x . If $|\mathcal{C}_F| = 1$, it trivially cannot distinguish 10 classes. So, Lemma 1 holds.

Lemma 2. *There exists an adaptive codebook function $AC(x, \mathcal{P})$ that maintains the Cluster Assignment Property under L_∞ perturbations of $\epsilon < \frac{w}{2}$.*

For an image I , let your algorithm consist of the following.

1. Find $\text{argmin}_{c_x \in I, c_y \in I} c_y - c_x$, or in other words, the largest gap between any two colors c_x and c_y in the image.
2. Let c_b refer to the midpoint $\frac{c_x + c_y}{2}$.
3. Assign all pixels in the input image $x[i, j] < c_b$ to c_x and all pixels in the input image $x[i, j] > c_b$ to c_y .

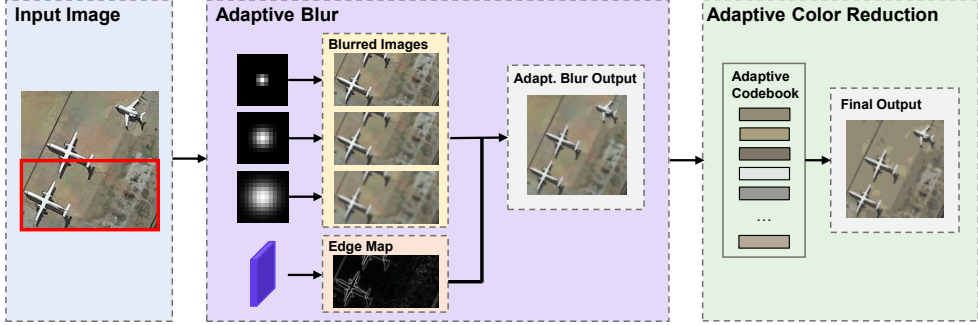


Figure 2: *Essential Features* pipeline. *Essential Features* first applies adaptive blurring with different blur kernels depending on the edge response map. *Essential Features* then applies adaptive color reduction to a codebook tailored to the per-image content.

Under perturbations with $\epsilon < \frac{w}{2}$, the algorithm guarantees the property that the assignment of pixels to c_1 and c_2 remains constant. This is because there must be a gap of $\geq \frac{w}{2}$ between the two clusters originally assigned to c_1 and c_2 that c_b will fall between. Splitting down the middle could shift c_1 and c_2 but will preserve the assignment. So, Lemma 2 holds.

By Lemma 1 and Lemma 2, the theorem holds. □

3.2 Design Considerations

The above proof-of-concept introduces two key principles that color reduction defenses must balance: (i) *representation*, i.e. the defense’s ability to consider properties of the data and to faithfully reconstruct its essential features, and (ii) *separability*, i.e. the ability for an attacker to change a pixel’s color to a create an unwanted feature. Our per-image adaptive transformation aims to achieve both properties even when they cannot be achieved on a dataset-wide scale.

By better balancing the representation-separability trade-off, we can more aggressively reduce the color space, constraining the attack space by forcing the adversary to move regions of similar colors in the same direction to change their color. Choosing the codebook adaptively per-image does allow the adversary to influence the color palette with their perturbations, so we will leverage spatial correlation to smooth the input in a semantically-aware way before applying color reduction. This further constrains the attack space by forcing the adversary to make larger changes in spatial regions to survive the transform. We also expect results with *Essential Features* to improve on larger resolution datasets, where more smoothing can be applied without removing the semantic features.

4 Approach

Per Section 3, *Essential Features* aims to cut down the attack surface by applying adaptive, content-aware preprocessing. This consists of two major phases: 1) *adaptive blurring*, which applies preliminary cleanup of adversarial noise by using edge-aware blurring and 2) *adaptive color reduction*, which reduces the color space with an adaptive, per-image codebook. The pipeline is depicted in Fig. 2.

4.1 Adaptive Gaussian Blurring

Applying Gaussian blurring removes high frequency changes an adversary may attempt to add [27, 10] but may additionally blur edges that make up the shape of the object in question or other fine details. As such, there is a fundamental trade-off between cleaning up noise and preserving important edge and shape features, which are important features

in human vision [28]. To accomplish both goals, we motivate and propose an edge-aware adaptive blur, which attempts to preserve pertinent edges by selecting smaller kernels in areas with a high edge map response and selecting larger kernels in areas with roughly the same color to limit an adversary’s ability to add misleading features.

4.1.1 Computing Edges

We compute channel-wise edge response maps by taking the gradient magnitude of the standard Sobel [29] filters in the x and y directions. We then normalize it by dividing by 1140.4 in the image range of [0, 255], which is the maximal attainable Sobel magnitude.

We choose Sobel edge response maps over the use of Canny Edge Detection [30] for two reasons. First, Sobel’s finer-grained response maps allow differential response to weak edges such as textures in a patch of grass that may be picked up versus the pertinent edges that make up the outline of the main object. Second, we want an efficient computation for adversarial training.

4.1.2 Adaptive Kernel Thresholding

Once an edge response map has been computed, we then adaptively blur the image with different Gaussian kernels based on the edge responses. To preserve the edges, we want to apply little blur on strong edge pixels and large blur on pixels in the middle of an object.

Specifically, given a set of m decreasing kernel sizes z_1, z_2, \dots, z_m to choose from and a set of increasing thresholds t_1, t_2, \dots, t_{m-1} we choose a blur level according to the edge response map. If the edge response at a pixel is $< t_1$, we apply z_1 . Otherwise, let t_i be the largest threshold the edge response is greater than. We then blur this pixel with z_{i+1} . Thus, in an area with no edges, we apply the most blur, and then for stronger and stronger edges, we apply less and less blur. This process is applied on each color channel separately.

These thresholds are set based on the selected threat model. We will generally use the highest blur on edges less than or equal to the strength of edge increase allowed by the threat model; to have some protection on small edges that the adversary amplified, we double that threshold to set the range of edges that use the middle blur. Note that one weakness of this approach is that if the important edges in the dataset are not significantly stronger the edges an adversary can add within the perturbation budget, it becomes harder to distinguish properly.

4.1.3 Summary

We apply adaptive, edge-aware blurring to clean up the image before passing it to color reduction. The result of this is that the adversary’s ability to influence the palette is limited to shifting large portions of the image in a similar direction or placing the perturbation on the existing strong edges.

4.2 Adaptive Color Reduction

The goal of this transformation is to reconstruct the input as faithfully as possible (high representation) with separable colors (high separability). We select the codebook colors per-image basis rather than per-dataset basis as in prior work [12]. This can be formulated as the following optimization problem, where T_C takes each pixel in an image x and sets it to the nearest color in the cluster palette C , and where d is the minimum distance between any two clusters:

$$\begin{aligned} \operatorname{argmin}_C & \|T_C(x) - x\|_2 \\ \text{s.t. } & \forall_i \forall_j \|C_i - C_j\|_2 > d \end{aligned} \tag{5}$$

4.2.1 Selecting an Adaptive Codebook

We apply an adaptive per-image color reduction transform. We modify the “Fast” k -means color reduction process seen in Jalalpour et al. [19], where k -means clustering is run on a thumbnail version of the image. k -means clustering finds centers of k clusters such that replacing each pixel in the image with the closest color in the set by Euclidean distance has a minimal reconstruction error.

We modify k -means to select the number of clusters k adaptively based on the content of the image and to enforce a minimum separability between clusters. This helps the algorithm adjust when some classes require more colors than others. We first change the initialization of clusters; rather than using random initialization like the original algorithm, we bin the color space into $b \times b \times b$ cubes and initialize a cluster in the center of each cube that contains a color of any pixel in the image. This allows for good initial representation. Then, to enforce separability, we add a final stage after the clustering to pare down the cluster list by greedily iterating over the cluster list and accepting colors only if they are at least d away from all other previously accepted colors.

4.2.2 Summary

We apply a variant of k -means clustering that selects both the colors and number of colors in the codebook adaptively. The effect of the adaptive color reduction is that it makes it harder for an adversary to add a lot of new colors, as this transformation will attempt to simplify the color palette to just the most representative colors. The adversary is now restricted to shifting larger amounts of pixels in the same cluster in the same direction or by changing the cluster assignment of pixels near the boundary, of which we hope there are few.

5 Experiments

We test *Essential Features* experimentally to answer these research questions:

- Q.1 How well does *Essential Features* defend against L_2 bounded attacks?
- Q.2 How well does *Essential Features* defend against L_∞ bounded attacks?
- Q.3 Under what conditions does *Essential Features* work well or not?

To answer these, we test *Essential Features* against other adversarial training baselines and on a variety of attacks, including adaptive PGD [20] and black-box [31] attacks. We train *Essential Features* with ATTA [26] (an efficient adversarial training method) and compare against vanilla ATTA trained models. Summary research highlights are shown in the answers below.

- A.1 We find significant improvements in L_2 robustness over adversarial training baselines in Fashion MNIST, CIFAR-10, RESISC45, and Imagenette. While Chen et al. [12] offers comparable robustness in the simpler MNIST and Fashion MNIST datasets, *Essential Features* significantly outperforms Chen et al. on CIFAR-10, RESISC45, and Imagenette.
- A.2 We find that *Essential Features* improves the L_2 robustness over adversarial training baselines and Chen et al. in higher resolution datasets like RESISC45 and Imagenette. *Essential Features* performs comparably to our baselines and Chen et al. on lower resolution datasets.
- A.3 As shown in A.2, *Essential Features* works best on higher resolution datasets where more detail is provided and more aggressive adversarial cleanup can be applied without losing the essential features of the original image. We also find that *Essential Features* performs more reliably on more “natural” datasets that do not rely on sharp edges in certain areas to distinguish between classes, such as the numbering on speed limit signs in GTSRB.

5.1 Experimental Setup

We describe the main points of our experimental setup. Additional hyperparameters and details are included in the supplement (Section A).

5.1.1 Datasets and Models

We test our *Essential Features* approach against the MNIST [32], Fashion-MNIST [33], CIFAR-10 [13], GTSRB [34], RESISC45 [14], and Imagenette datasets [15]. Like Chen et al. [12], we remove all images with an average intensity of 50 from GTSRB. We use ATTA [26] as an efficient adversarial training technique. For MNIST and Fashion-MNIST, we use the MNIST architecture used in prior work [20]. For CIFAR-10 and GTSRB, we use the Wide ResNet 34-10 [35] architecture commonly used in adversarial training techniques [20, 25, 26]. For RESISC45 and Imagenette, we use ResNet-34 [36].

5.1.2 Attack Details

For our L_∞ PGD-based attacks our setup is similar to prior work [12]. Specifically, for MNIST, we use $\epsilon = 0.3$ and 100 steps of size 0.01. For Fashion-MNIST, we use $\epsilon = 0.1$ and 100 steps of size 0.01. For CIFAR-10, we test with $\epsilon = 0.031$ and 40 steps of size 0.007. For GTSRB and RESISC45, we use $\epsilon = 0.031$ and 40 steps of size 0.007. For Imagenette, we test with $\epsilon = 4/255$ and 10 steps of size 1/255.

For L_2 attacks, we adjust the ϵ values by setting them equal to what the L_2 distance would be for an attack that used the corresponding L_∞ budget on each pixel. For example, for CIFAR-10, perturbing each value by $\epsilon = 8/255$ would have a distortion of $8/255 \cdot \sqrt{32 \cdot 32 \cdot 3} = 1.74$, so we set this $L_2 \epsilon$ to 1.74. For MNIST, Fashion-MNIST, CIFAR-10, GTSRB, RESISC45, and Imagenette, we use step sizes of 0.1, 0.5, 0.05, 0.05, 0.35, and 0.85 respectively.

For adaptive attacks, we apply backwards pass differentiable approximation (BPDA) [11]. For the adaptive color reduction, we set $g(x)$ to the identity function. For adaptive blur, we differentiate exactly under the assumption that the choice of kernels will remain constant. For attacking Chen et al. [12], we use their proposed adaptive attack. We discuss alternatives in the supplement (Section B).

We also modify PGD to return the attack from the step with the highest loss rather than simply returning the attack from the last step. This helps improve the attack success rate on models with *Essential Features* without noticeably impacting the baseline evaluation. All future PGD references assume this change.

We also test a black-box soft-label attack known as Square Attack [31] to provide a different style of attack and expose potential gradient masking issues [37, 38]. We use 1000 iterations. For efficiency, we test on a 500 image subset.

5.1.3 *Essential Features* Transformation Details

For adaptive blurring, on the 32×32 datasets (CIFAR-10 and GTSRB), we use the smallest three possible kernel widths of $\{5, 3, 1\}$. A kernel of 5 is still a large amount of blur however, covering over 15% of the image length. MNIST and Fashion-MNIST are even smaller, so we use $\{3, 1, 1\}$. For RESISC45, we use kernels of size $\{13, 7, 3\}$, which is about 5%, 2.5% and 1% of the 256 image length. For Imagenette, we use $\{11, 5, 3\}$ to maintain similar ratios as RESISC45. The kernels use the default standard deviation from OpenCV.

We set the kernel thresholds equal to $\{20, 40\}$ for each dataset except for Imagenette, which we reduce to $\{10, 20\}$ given the smaller epsilon bounds. The $\{20, 40\}$ thresholds ensure that the strength of edges an adversary could apply under the L_∞ bounds of CIFAR-10, GTSRB, and RESISC45 would be below these values (and similarly with $\{10, 20\}$ for Imagenette).

For our color reduction process, we bin the color space up into cubes of length $b = 16$ for cluster initialization. We set 32×32 to be the thumbnail size for Fast k -means [19]. Then, when paring down the cluster list, we enforce a minimum distance d equal to 3x

Table 1: White-box robustness results on more complex color datasets. We find that *Essential Features* improves L_2 and L_∞ robustness on higher resolution datasets (RESISC45, Imagenette) and improves L_2 robustness on CIFAR-10.

| Dataset | Model | Accuracy | Robustness (L_2 PGD) | Robustness (L_∞ PGD) |
|------------|--------------------------|---------------|-------------------------|------------------------------|
| CIFAR-10 | ATTA | 85.43% | 20.15% | 51.72% |
| | ATTA + EF at Test Time | 82.11% | 24.92% | 47.73% |
| | ATTA + Chen at Test Time | 84.73% | 26.42% | 52.91% |
| | ATTA Retrained with EF | 84.52% | 38.46% | 51.97% |
| GTSRB | ATTA | 92.47% | 57.28% | 78.24% |
| | ATTA + EF at Test Time | 89.22% | 57.20% | 71.93% |
| | ATTA + Chen at Test Time | 92.31% | 59.82% | 81.16% |
| | ATTA Retrained with EF | 90.32% | 57.71% | 73.25% |
| RESISC45 | ATTA | 82.00% | 12.09% | 43.89% |
| | ATTA + EF at Test Time | 62.02% | 20.04% | 27.22% |
| | ATTA + Chen at Test Time | 81.89% | 16.36% | 46.27% |
| | ATTA Retrained with EF | 88.24% | 52.44% | 53.33% |
| Imagenette | ATTA | 93.58% | 65.50% | 75.97% |
| | ATTA + EF at Test Time | 90.93% | 65.89% | 74.93% |
| | ATTA + Chen at Test Time | 93.45% | 70.83% | 78.70% |
| | ATTA Retrained with EF | 95.34% | 72.28% | 80.71% |

the size of ϵ . This way, should an adversary attempt to take two pixels at the center of two clusters and switch them, there are two radii of ϵ plus and ϵ length of buffer between them, to minimize the number of pixels where the adversary could choose which cluster they belong to.¹

5.2 Experimental Results

Our results on *Essential Features* are summarized in Table 1 and Table 2. We show results on four models: 1) the regularly trained ATTA baseline, 2). The PGD parameters are those specified in Section 5.1. We analyze these results with our three research questions above in mind in the following subsections.²

5.2.1 L_2 Robustness

We find that adversarial robustness against L_2 attacks improves significantly with *Essential Features* retrained models compared to vanilla ATTA on CIFAR-10 (20.15% to 38.46%), RESISC45 (12.09% to 52.44%), and Imagenette (65.50% to 72.28%). *Essential Features* also outperforms Chen et al. [12] on these datasets.

The L_2 robustness does not significantly improve with *Essential Features* on GTSRB. We argue in Section 5.3 that this is due to the reliance on small, high frequency differences in a few key areas to distinguish between multiple classes.

We find that on MNIST and Fashion-MNIST, discretization transforms are generally better when added on to existing models than with retraining. We suspect with the larger perturbation bounds when retraining the adversary may have too much influence on the color palette to learn an optimal boundary. When adding *Essential Features* to a vanilla

¹Note that for MNIST, with an ϵ of 0.3, this works out to be 230 / 255. Thus, we tweak the coalescing algorithm to avoid choosing a cluster that would automatically rule out the ability to pick a second cluster. If no such pair of clusters obey this distance, we simply choose the farthest two apart.

²We found other settings such as adding EF or Chen et al. [12] to natural models or retraining on Chen et al. [12] to not provide any significant improvement in any setting. We discuss other settings in the supplement (Section C).

Table 2: White-box robustness results on simpler grayscale datasets. Adding *Essential Features* at test time improves L_2 and L_∞ robustness over vanilla ATTA, while retraining improves L_∞ robustness on Fashion-MNIST. We show in the supplement (Section D) that Chen et al.’s L_2 robustness is likely overstated; once adjusted, Chen et al. performs comparably to *Essential Features*.

| Dataset | Model | Accuracy | Robustness (L_2 PGD) | Robustness (L_∞ PGD) |
|-------------------|--------------------------|---------------|----------------------------|---------------------------------|
| MNIST | ATTa | 96.53% | 0.00% | 87.47% |
| | ATTa + EF at Test Time | 96.29% | 13.89% | 92.76% |
| | ATTa + Chen at Test Time | 96.30% | 28.75% | 93.85% |
| | ATTa Retrained with EF | 98.43% | 0.00% | 91.00% |
| Fashion- MNIST | ATTa | 81.74% | 13.82% | 69.80% |
| | ATTa + EF at Test Time | 81.27% | 30.15% | 70.61% |
| | ATTa + Chen at Test Time | 78.95% | 43.41% | 66.69% |
| | ATTa Retrained with EF | 82.06% | 23.37% | 71.54% |

ATTa model, we find that L_2 robustness increases with *Essential Features* compared to without.

On MNIST and Fashion-MNIST, Chen et al. [12] performs better on white-box attacks when adding the transform than *Essential Features*, but we find in the supplement (Section D) that Square Attack greatly reduces its performance (13.0% for MNIST, 27.8% for Fashion-MNIST on 500 samples), suggesting that the adaptive attack to Chen et al. [12] is overestimating the robustness. The Square Attack numbers on Chen et al. [12] are comparable to *Essential Features*’s performance. Note that there were no other cases in which our 500 image Square Attack test performed notably better than PGD (see supplement Section D).

5.2.2 L_∞ Robustness

We find that on higher resolution datasets *Essential Features* improves the L_∞ robustness over vanilla ATTA (43.89% to 53.33% on RESISC45, 75.97% to 80.71% on Imagenette) and over Chen et al. [12]. These datasets benefit from having more detail and thus more ability to blur and color reduce aggressively without removing essential features of the original image.

On GTSRB, we find that the robustness gets slightly worse. Similarly to the L_2 analysis, we explain this in Section 5.3 to be due to its reliance on small, high frequency differences in a few key areas to distinguish between multiple classes.

We find on MNIST and Fashion-MNIST that adversarial training with *Essential Features* improves the L_∞ robustness over vanilla ATTA models. We also find that on Fashion-MNIST *Essential Features* performs better than Chen et al. [12]. On the simple MNIST dataset where black and white discretization works extremely well, *Essential Features* performs comparably to Chen et al. [12].

On L_∞ attacks, we found that PGD performed at least comparably to our 500 image Square Attack test in all cases (see supplement Section D).

5.3 Analysis

In this section, we explore the conditions under with *Essential Features* performs well. We have already seen in Section 5.2 that *Essential Features* performs better on higher resolution datasets. We now examine an example of how the L_2 attack space is restricted in RESISC45, analyze the lack of improvement on GTSRB, and look at the perceptibility of L_∞ attacks. We also include ablations in the supplement (Section E) that evaluate just adaptive blurring or color reduction.



Figure 3: L_2 attack example on RESISC45 ATTA baseline. L_2 attacks consisting of isolated pixels with large perturbations no longer work as well. **Left:** an original image of an island from RESISC45 with a box of interest drawn. **Center:** adversarial version, zoomed in, where black dot and pink perturbations are clearly visible. **Right:** *Essential Features* transformed version that removed the black and pink perturbations.

5.3.1 L_2 Results

The way we set the L_2 bounds to include the L_∞ space in comparison to means that the space of L_∞ is a subset of the L_2 attack space. Thus, we should always expect the L_2 robustness to be less than the L_∞ robustness.

It is then interesting to consider why the relative increases of robustness under *Essential Features* improves more dramatically under L_2 than under L_∞ . In the case of RESISC45, the L_2 robustness is nearly brought to the L_∞ robustness (52.44% vs. 53.33%), which would mean that the added space in the L_2 domain is barely providing any additional attacks.

We understand this to be a consequence of *Essential Features*’s design. In particular, if the adaptive blur can eliminate isolated pixel changes in non-edge regions well enough that color reduction sends it to the correct cluster, we can undo the effects of that perturbed pixel. As an example, we show in Fig. 3 a perturbed L_2 attack of an island from the RESISC45 against a vanilla ATTA model. We find that the attack left some isolated but noticeable black and pink perturbations. However, when applying *Essential Features*, these individual changes disappeared, showing the types of attacks that are no longer available.

5.3.2 GTSRB Results

We now analyze our GTSRB results as one of the datasets where *Essential Features* did not improve performance in any setting. We observe that the baselines already perform fairly well, making further improvements difficult. In addition, we found several examples of attacks that would cause enough confusion to possibly mess up a human’s decision because of their blurry nature and inherent reliance on particular features at a couple of key spots.

We show a couple of L_2 and L_∞ examples in Fig. 4 where the attack wiped away some of the distinguishing features in key parts of image (such as the numbering on speed limit signs). Such attacks will be hard for any defense to defend against, and thus explains why *Essential Features* appears to perform better on datasets with more naturally occurring images such as CIFAR-10 or RESISC45 that do not have as much dependency on small, specific features.

5.3.3 Perceptibility

We now test if attacks on *Essential Features* models are more perceptible than vanilla ATTA models, given that our transformation makes it harder to attack without changing regions of color-wise and spatial locality together. We first measure the SSIM [39] of L_∞ attacked images from a vanilla ATTA model and our *Essential Features* trained ATTA model against the original, where higher SSIM means more similarity to the original.

We tested on the 4 color datasets and found on average there was not a significant change from the average SSIM on vanilla ATTA attacks versus the average SSIM on *Essential Features* attacks (0.946 vs. 0.944 for CIFAR-10, 0.927 vs. 0.933 for GTSRB, 0.899 vs. 0.877 for RESISC45, 0.955 vs. 0.963 for Imagenette). The low resolution is a likely



Figure 4: Example attacks on *Essential Features* GTSRB model where the attacked image appears to be a different class or ambiguous. **Left:** L_∞ attack that looks like it may be a 50 km/hr. Actual GT label: 80 km/hr. **Left Center:** L_∞ attack that has little detail, and could feasibly be a wild animal crossing sign. Actual GT label: Winding Road. **Center Right:** L_2 attack that looks like a 50 km/hr. Actual GT label: 30 km/hr. **Right:** L_2 attack that has very little detail inside. Actual GT label: Bike crossing.



Figure 5: SSIM does not necessarily capture the change in perceptibility on *Essential Features* model attacks. **Left:** original image. **Center:** vanilla ATTA model attack. SSIM: 0.893. **Right:** *Essential Features* trained ATTA model attack. SSIM: 0.868.

explanation for CIFAR-10 and GTSRB, and for the higher resolution datasets, we qualitatively find that the *Essential Features* attacks often exhibit grid like blob perturbations that are not necessarily reflected in SSIM in large areas of similar color. We show in Fig. 5 an example of an *Essential Features* attack with clear perturbations but a similar SSIM score as a vanilla ATTA attack. This shows that neither SSIM nor L_∞ necessarily capture the true increase of perceptibility. We leave more exploration to future work.

6 Conclusion

We propose *Essential Features*, a content adaptive pixel discretization defense to improve model robustness. Compared to using a fixed dataset-wide codebook strategy [12], we find that using a per-image approach can constrain the attack space on additional datasets and improve L_2 and L_∞ robustness, particularly on higher resolution datasets. This work demonstrates the utility of an adaptive approach to better balance representation and separability and motivates the continued development of adaptive preprocessing defenses.

Acknowledgements

This material is based on work supported by DARPA under agreement number 885000, the National Science Foundation (NSF) Grants 1646392 and 2039445, MIDAS at the University of Michigan, and Ford. The U.S. Government is authorized to reproduce and distribute reprints for Governmental purposes notwithstanding any copyright annotation thereon. The views and conclusions contained herein are those of the authors and should not be interpreted as necessarily representing the official policies or endorsements, either expressed or implied, of the research sponsors or the U.S. Government.

References

[1] A. Athalye, L. Engstrom, A. Ilyas, and K. Kwok, “Synthesizing robust adversarial examples,” *arXiv preprint arXiv:1707.07397*, 2017.

- [2] N. Carlini and D. Wagner, “Towards evaluating the robustness of neural networks,” in *2017 ieee symposium on security and privacy (sp)*. IEEE, 2017, pp. 39–57.
- [3] K. Eykholt, I. Evtimov, E. Fernandes, B. Li, A. Rahmati, C. Xiao, A. Prakash, T. Kohno, and D. Song, “Robust Physical-World Attacks on Deep Learning Visual Classification,” in *Computer Vision and Pattern Recognition (CVPR)*, June 2018.
- [4] I. J. Goodfellow, J. Shlens, and C. Szegedy, “Explaining and harnessing adversarial examples,” *arXiv preprint arXiv:1412.6572*, 2014.
- [5] A. Kurakin, I. Goodfellow, and S. Bengio, “Adversarial examples in the physical world,” *arXiv preprint arXiv:1607.02533*, 2016.
- [6] C. Szegedy, V. Vanhoucke, S. Ioffe, J. Shlens, and Z. Wojna, “Rethinking the inception architecture for computer vision,” in *Proceedings of the IEEE conference on computer vision and pattern recognition*, 2016, pp. 2818–2826.
- [7] N. Das, M. Shanbhogue, S.-T. Chen, F. Hohman, L. Chen, M. E. Kounavis, and D. H. Chau, “Keeping the bad guys out: Protecting and vaccinating deep learning with jpeg compression,” *arXiv preprint arXiv:1705.02900*, 2017.
- [8] G. K. Dziugaite, Z. Ghahramani, and D. M. Roy, “A study of the effect of jpg compression on adversarial images,” *arXiv preprint arXiv:1608.00853*, 2016.
- [9] C. Guo, M. Rana, M. Cisse, and L. Van Der Maaten, “Countering adversarial images using input transformations,” *arXiv preprint arXiv:1711.00117*, 2017.
- [10] W. Xu, D. Evans, and Y. Qi, “Feature squeezing: Detecting adversarial examples in deep neural networks,” *arXiv preprint arXiv:1704.01155*, 2017.
- [11] A. Athalye, N. Carlini, and D. Wagner, “Obfuscated gradients give a false sense of security: Circumventing defenses to adversarial examples,” *arXiv preprint arXiv:1802.00420*, 2018.
- [12] J. Chen, X. Wu, V. Rastogi, Y. Liang, and S. Jha, “Towards understanding limitations of pixel discretization against adversarial attacks,” in *2019 IEEE European Symposium on Security and Privacy (EuroS&P)*. IEEE, 2019, pp. 480–495.
- [13] A. Krizhevsky, “Learning multiple layers of features from tiny images,” 2009.
- [14] G. Cheng, J. Han, and X. Lu, “Remote sensing image scene classification: Benchmark and state of the art,” *Proceedings of the IEEE*, vol. 105, no. 10, pp. 1865–1883, 2017.
- [15] J. Howard, “Imagenette.” [Online]. Available: <https://github.com/fastai/imagenette/>
- [16] A. Prakash, N. Moran, S. Garber, A. DiLillo, and J. Storer, “Deflecting adversarial attacks with pixel deflection,” in *Proceedings of the IEEE conference on computer vision and pattern recognition*, 2018, pp. 8571–8580.
- [17] A. Athalye and N. Carlini, “On the robustness of the cvpr 2018 white-box adversarial example defenses,” *arXiv preprint arXiv:1804.03286*, 2018.
- [18] B. Liang, H. Li, M. Su, X. Li, W. Shi, and X. Wang, “Detecting adversarial image examples in deep neural networks with adaptive noise reduction,” *IEEE Transactions on Dependable and Secure Computing*, 2018.
- [19] Y. Jalalpour, L.-Y. Wang, R. Feng, and W.-c. Feng, “Leveraging image processing techniques to thwart adversarial attacks in image classification,” in *2019 IEEE International Symposium on Multimedia (ISM)*. IEEE, 2019, pp. 184–1847.
- [20] A. Madry, A. Makelov, L. Schmidt, D. Tsipras, and A. Vladu, “Towards deep learning models resistant to adversarial attacks,” *arXiv preprint arXiv:1706.06083*, 2017.

- [21] A. Kurakin, I. Goodfellow, and S. Bengio, “Adversarial machine learning at scale,” *arXiv preprint arXiv:1611.01236*, 2016.
- [22] A. Shafahi, M. Najibi, M. A. Ghiasi, Z. Xu, J. Dickerson, C. Studer, L. S. Davis, G. Taylor, and T. Goldstein, “Adversarial training for free!” in *Advances in Neural Information Processing Systems*, 2019, pp. 3358–3369.
- [23] E. Wong, L. Rice, and J. Z. Kolter, “Fast is better than free: Revisiting adversarial training,” *arXiv preprint arXiv:2001.03994*, 2020.
- [24] D. Zhang, T. Zhang, Y. Lu, Z. Zhu, and B. Dong, “You only propagate once: Accelerating adversarial training via maximal principle,” in *Advances in Neural Information Processing Systems*, 2019, pp. 227–238.
- [25] H. Zhang, Y. Yu, J. Jiao, E. P. Xing, L. E. Ghaoui, and M. I. Jordan, “Theoretically principled trade-off between robustness and accuracy,” *arXiv preprint arXiv:1901.08573*, 2019.
- [26] H. Zheng, Z. Zhang, J. Gu, H. Lee, and A. Prakash, “Efficient adversarial training with transferable adversarial examples,” in *Proceedings of the IEEE/CVF Conference on Computer Vision and Pattern Recognition*, 2020, pp. 1181–1190.
- [27] R. S. Raju and M. Lipasti, “Blurnet: Defense by filtering the feature maps,” in *2020 50th Annual IEEE/IFIP International Conference on Dependable Systems and Networks Workshops (DSN-W)*. IEEE, 2020, pp. 38–46.
- [28] A. M. Treisman and N. G. Kanwisher, “Perceiving visually presented objects: recognition, awareness, and modularity,” *Current opinion in neurobiology*, vol. 8, no. 2, pp. 218–226, 1998.
- [29] G. Bradski and A. Kaehler, *Learning OpenCV: Computer vision with the OpenCV library.* O'Reilly Media, Inc., 2008.
- [30] J. Canny, “A computational approach to edge detection,” *IEEE Transactions on pattern analysis and machine intelligence*, vol. 8, no. 6, pp. 679–698, 1986.
- [31] M. Andriushchenko, F. Croce, N. Flammarion, and M. Hein, “Square attack: a query-efficient black-box adversarial attack via random search,” in *European Conference on Computer Vision*. Springer, 2020, pp. 484–501.
- [32] Y. LeCun, L. Bottou, Y. Bengio, and P. Haffner, “Gradient-based learning applied to document recognition,” *Proceedings of the IEEE*, vol. 86, no. 11, pp. 2278–2324, 1998.
- [33] H. Xiao, K. Rasul, and R. Vollgraf, “Fashion-mnist: a novel image dataset for benchmarking machine learning algorithms,” *arXiv preprint arXiv:1708.07747*, 2017.
- [34] J. Stallkamp, M. Schlipsing, J. Salmen, and C. Igel, “Man vs. computer: Benchmarking machine learning algorithms for traffic sign recognition,” *Neural Networks*, vol. 32, pp. 323–332, 2012. [Online]. Available: <http://www.sciencedirect.com/science/article/pii/S0893608012000457>
- [35] S. Zagoruyko and N. Komodakis, “Wide residual networks,” *arXiv preprint arXiv:1605.07146*, 2016.
- [36] K. He, X. Zhang, S. Ren, and J. Sun, “Deep residual learning for image recognition,” in *Proceedings of the IEEE conference on computer vision and pattern recognition*, 2016, pp. 770–778.
- [37] N. Carlini, A. Athalye, N. Papernot, W. Brendel, J. Rauber, D. Tsipras, I. Goodfellow, A. Madry, and A. Kurakin, “On evaluating adversarial robustness,” *arXiv preprint arXiv:1902.06705*, 2019.

- [38] F. Tramer, N. Carlini, W. Brendel, and A. Madry, “On adaptive attacks to adversarial example defenses,” *arXiv preprint arXiv:2002.08347*, 2020.
- [39] Z. Wang, A. C. Bovik, H. R. Sheikh, and E. P. Simoncelli, “Image quality assessment: from error visibility to structural similarity,” *IEEE transactions on image processing*, vol. 13, no. 4, pp. 600–612, 2004.
- [40] M. Sharif, S. Bhagavatula, L. Bauer, and M. K. Reiter, “Accessorize to a crime: Real and stealthy attacks on state-of-the-art face recognition,” in *Proceedings of the 2016 ACM SIGSAC Conference on Computer and Communications Security*, ser. CCS ’16, 2016, p. 1528–1540.

A Additional Experimental Details

A.1 Training Details

For MNIST and Fashion-MNIST, we train natural models for 40 epochs with a learning rate of 0.01 for 35 epochs and 0.001 for the remaining. We use a batch size of 128, weight decay of 2e-4, and 0.9. we use settings as in [26] with 100 epochs and a learning rate division of 10 at epochs 55, 75, and 90. For the ATTA-based models, we use a batch size of 64, train for 60 epochs without resetting the perturbations, momentum 0.9, starting learning rate of $0.1 \cdot 1/64$ and weight decay of $2e-4 \cdot 64$, and we divide the learning rate by 10 after 55 epochs³. The training time attacks were PGD-40 with a step size of 0.01 and $\epsilon = 0.3$ for MNIST and PGD-20 with a step size of 0.01 and $\epsilon = 0.1$ for Fashion-MNIST, following prior work [12].

For CIFAR-10 and GTSRB, we train natural models the same as MNIST but with the learning rate 10x as high (starting at 0.1). For ATTA-based models, we use 38 epochs, a perturbation reset of 10 epochs, a starting learning rate of $0.1 \cdot 1/64$ with a division by 10 at epochs 30 and 35, and $2e-4 \cdot 64$ for weight decay, following prior work [26] (see footnote 3). The training time attacks were PGD-7 with a step size of $2/255 = 0.007$ and ϵ of $8/255 = 0.031$.

For RESISC45, we use the same settings as MNIST for natural training. For ATTA-based models, we use 40 epochs, a perturbation reset of 10 epochs, a starting learning rate of $0.1 \cdot 1/64$ with a division by 10 at epochs 30 and 35, and $2e-4 \cdot 64$ for weight decay. The training time attacks were PGD-10 attacks with a step size of $2/255 = 0.007$ and an ϵ of $8/255 = 0.031$.

For Imagenette, we use the same settings as MNIST and RESISC45 for natural training. For ATTA-based models, we use the same settings as RESISC 45 except the training time attacks were PGD-10 attacks with a step size of $1/255 = 0.004$ and an ϵ of $4/255 = 0.0157$.

Additionally, for ATTA experiments on GTSRB, RESISC45, and Imagenette, we save out intermediate results rather than caching the entire dataset in memory as the original code does due to memory concerns. Following previous work [20, 26], we apply random horizontal flipping and random cropping data augmentation. For CIFAR-10, as in prior work [20, 26], we apply padding of 4 pixels on each side and randomly crop back to 32×32 . For RESISC45 and Imagenette, we apply padding of 2 pixels on each side and randomly crop back to the original resolution.

A.2 Essential Features Details

For k -means color reduction, as in Jalalpour et al. [19], we approximate the choice of colors on a smaller thumbnail image before assigning the original image’s colors to that palette. We downsize the image to a resolution of 32×32 for the thumbnail version. We use OpenCV’s area interpolation method. We run k -means clustering for 20 iterations.

³We confirmed through correspondence with the original authors that there was an additional batch size division in the code. Adjusting the values as we have replicates the original code’s behavior for a learning rate input of 0.1 and weight decay of 2e-4.

A.3 Chen et al. Details

For experiments involving Chen et al. [12], on common datasets we take the codebook settings from the most robust settings from the original paper. The specific parameters are k , the number of codewords, and r , a distance parameter. For MNIST and Fashion-MNIST, we use $k = 2$ and $r = 0.6$ (in [0-1] image range). For CIFAR-10 and RESISC45, we use $k = 300$ and $r = 16$ (in [0-255] image range), and for GTSRB and Imagenette we use $k = 500$ and $r = 16$.

For the adaptive attack settings, as in the original paper [12], we use a value of 10 for their attack parameter α on MNIST and Fashion-MNIST and a value of 0.1 for other datasets.

A.4 Dataset Details

For GTSRB, similar to prior work we crop and scale all images to 32×32 [12, 3]. Our specific process entails cropping the image at the given annotation region-of-interest (ROI) coordinates included with the data download, padding the crop to a square and resizing the square to 32×32 . This way, the crops can be used in a consistent 32×32 size without changing the distortion or aspect ratio of the images.

B Alternative Adaptive Attacks

We explored a few other adaptive white-box attack strategies but found them to be no better than using the identity function for color reduction and differentiating through the adaptive blur with the assumption the choice of kernel remains static, as described in the main paper. The first alternative attack tried adding an additional term to the attack objective function to maximize the average Sobel map response to encourage the adversary to add edges. We note that due to edge thresholding in the adaptive kernel selection (Section 4.1.2) the attacker is not able to add very much to the edge response within small L_∞ ball limits, which limits the ability to attack the image by adding lots of strong edges. The second alternative attack tried to add a Non Printability Score [40] to encourage the attack to use very few colors. We tried using the set of colors used in [3] and from the palette generated by k -means on the original input image, but neither improved the attack success rate. Third, for the color reduction stage, we tried using the same approximation as Chen et al. [12] for the currently selected cluster at each step. However, initial testing found this to be less effective than the identity function, so we focus our evaluations with the identity function at the color reduction stage.

C Alternative Combinations of Training + Transforms

We include results on other training modes such as natural training, adding a transform to a naturally trained model, etc. in Table 3. We generally find these settings to be inferior to the ones in the main paper. We find that on CIFAR-10 adversarial training with Chen et al. [12] can perform slightly better on L_∞ attacks, but not by much (53.18% on adversarially trained Chen and 52.91% on a vanilla ATTA model with Chen at test time).

We also observe that unless we expect the data to have well split colors already (i.e. MNIST, Fashion-MNIST, GTSRB), models where the transform is merely added on at test time perform inferior to those that are retrained on the transform. This is consistent with the results from the main paper too. We also observe that adversarial training seems to be required for optimal performance.

D Black-box Evaluation

We include results on 500 samples of Square Attack [31] with 1000 iterations in Tables 4 and 5 for the settings presented in Tables 1 and 2 in the main paper and in the additional

combinations presented in Section C in the Supplement.

We do not see any large reductions on models with *Essential Features*, suggesting that our *Essential Features* adaptive attacks are reasonable. We observe that on CIFAR-10, GTSRB, RESISC45, and Imagenette, Square Attack never improves the attack on a model with *Essential Features* involved in any capacity except for RESISC45 adversarially trained with *Essential Features*, but the drop is less than 3% and within the noise of the 500 samples for Square Attack, suggesting that the adaptive attacks on *Essential Features* are good. The Square Attack numbers in several cases are also notably lower than the PGD numbers (such as the Natural + EF at Test Time and ATTA + EF at Test time settings for RESISC45 and Imagenette), suggesting that the adaptive attacks worked particularly well in these cases.

There are however some notable decreases on models with the Chen et al. [12] transform, for which we used the original paper’s adaptive attack. Notable decreases include MNIST on ATTA + Chen at Test Time (L_2 decreased from 28.75% to 13.0%) and Fashion-MNIST on ATTA + Chen at Test Time (L_2 decreased from 43.41% to 27.8%), as this decreases these models performance as originally seen from the PGD attacks. These results suggest that the adaptive attack for Chen et al. [12] could be further improved for a truer robustness estimate.

E Ablations

We include results on just adaptive blurring and just adaptive color reduction in Tables 6 and 7. We only test with the setting that adversarially trains the model with the transform.

We find that the full *Essential Features* appears better than just adaptive blurring in every case except for GTSRB, which had not improved over the baseline anyways. For adaptive color reduction, we can see that on the higher resolution datasets the full transform does the best on natural (88.24% vs 83.44% on RESISC45, 95.34% vs. 94.75% on Imagenette), L_2 PGD robustness (52.44% vs. 30.80% on RESISC45, 72.28% vs. 71.62% on Imagenette), and L_∞ PGD robustness (53.33% vs. 45.24% on RESISC45, 80.71% vs. 79.90% on Imagenette). The performance increase is particularly clear on RESISC45. The Imagenette gaps are not large, but that may be due to its smaller ϵ perturbation values. CIFAR-10 also benefits from the full pipeline on L_2 attacks compared to the adversarially trained model with *Essential Features* (29.45% vs. 38.46%).

It is perhaps not too surprising that on datasets with low resolution and well split colors already (i.e., MNIST, Fashion-MNIST, GTSRB) just adaptive color reduction performs similarly to the full transform. We also find that Square Attack [31] does not drastically reduce the accuracy compared to PGD, suggesting that the adaptive attacks are reasonable.

Table 3: White-box robustness results on alternative training modes. Generally, these modes achieve inferior performance to the versions reported in the main paper.

| Dataset | Model | Accuracy | Robustness (L_2 PGD) | Robustness (L_∞ PGD) |
|-------------------|-----------------------------|----------|----------------------------|---------------------------------|
| MNIST | Natural | 99.24% | 0.00% | 0.00% |
| | Natural + EF at Test Time | 99.05% | 0.00% | 74.99% |
| | Natural + Chen at Test time | 99.07% | 0.03% | 77.37% |
| | Natural Retrained with EF | 99.06% | 0.00% | 77.49% |
| | Natural Retrained with Chen | 99.17% | 0.04% | 79.79% |
| | ATTA Retrained with Chen | 98.47% | 0.17% | 91.60% |
| Fashion- MNIST | Natural | 92.51% | 0.01% | 1.99% |
| | Natural + EF at Test Time | 89.42% | 3.95% | 29.42% |
| | Natural + Chen at Test time | 81.96% | 7.90% | 40.56% |
| | Natural Retrained with EF | 90.54% | 5.86% | 32.79% |
| | Natural Retrained with Chen | 88.38% | 10.67% | 47.63% |
| | ATTA Retrained with Chen | 80.97% | 40.03% | 69.23% |
| CIFAR-10 | Natural | 94.59% | 0.00% | 0.00% |
| | Natural + EF at Test Time | 78.54% | 0.04% | 0.40% |
| | Natural + Chen at Test time | 90.40% | 0.00% | 0.00% |
| | Natural Retrained with EF | 91.11% | 0.75% | 2.46% |
| | Natural Retrained with Chen | 93.06% | 0.02% | 0.09% |
| | ATTA Retrained with Chen | 85.76% | 27.53% | 53.18% |
| GTSRB | Natural | 96.23% | 7.26% | 16.54% |
| | Natural + EF at Test Time | 92.27% | 18.21% | 31.21% |
| | Natural + Chen at Test time | 95.71% | 17.19% | 25.91% |
| | Natural Retrained with EF | 94.32% | 15.77% | 32.40% |
| | Natural Retrained with Chen | 95.53% | 19.34% | 27.66% |
| | ATTA Retrained with Chen | 88.08% | 57.83% | 76.02% |
| RESISC45 | Natural | 96.09% | 0.00% | 0.00% |
| | Natural + EF at Test Time | 54.11% | 2.88% | 1.60% |
| | Natural + Chen at Test time | 94.62% | 0.00% | 0.00% |
| | Natural Retrained with EF | 92.11% | 6.64% | 3.42% |
| | Natural Retrained with Chen | 95.51% | 0.00% | 0.00% |
| | ATTA Retrained with Chen | 74.13% | 8.22% | 43.71% |
| Imagenette | Natural | 98.98% | 0.026% | 0.00% |
| | Natural + EF at Test Time | 95.97% | 17.45% | 20.41% |
| | Natural + Chen at Test time | 98.29% | 0.79% | 0.66% |
| | Natural Retrained with EF | 98.55% | 24.66% | 30.85% |
| | Natural Retrained with Chen | 98.83% | 1.48% | 1.07% |
| | ATTA Retrained with Chen | 89.55% | 65.68% | 75.29% |

Table 4: Square Attack [31] results on 500 samples for the results provided in Table 1 and Table 2. Square Attack does not significantly reduce the robustness on any models with *Essential Features* involved, but does significantly reduce the L_2 robustness of the ATTA + Chen et al. models on MNIST and Fashion-MNIST.

| Dataset | Model | Robustness (L_2 Square on 500 Samples) | Robustness (L_∞ Square on 500 Samples) |
|-------------------|--------------------------|---|--|
| MNIST | ATTA | 0.8% | 83.8% |
| | ATTA + EF at Test Time | 11.6% | 86.0% |
| | ATTA + Chen at Test Time | 13.0% | 87.0% |
| | ATTA Retrained with EF | 16.6% | 89.8% |
| Fashion- MNIST | ATTA | 29.8% | 71.6% |
| | ATTA + EF at Test Time | 34.2% | 67.8% |
| | ATTA + Chen at Test Time | 27.8% | 66.6% |
| | ATTA Retrained with EF | 50.2% | 68.0% |
| CIFAR-10 | ATTA | 62.2% | 62.6% |
| | ATTA + EF at Test Time | 59.6% | 58.0% |
| | ATTA + Chen at Test Time | 62.0% | 58.8% |
| | ATTA Retrained with EF | 63.6% | 56.2% |
| GTSRB | ATTA | 59.0% | 81.0% |
| | ATTA + EF at Test Time | 60.0% | 81.0% |
| | ATTA + Chen at Test Time | 66.2% | 82.6% |
| | ATTA Retrained with EF | 62.0% | 73.8% |
| RESISC45 | ATTA | 46.8% | 63.8% |
| | ATTA + EF at Test Time | 37.8% | 33.8% |
| | ATTA + Chen at Test Time | 53.2% | 63.8% |
| | ATTA Retrained with EF | 60.8% | 50.6% |
| Imagenette | ATTA | 88.6% | 89.2% |
| | ATTA + EF at Test Time | 85.6% | 85.0% |
| | ATTA + Chen at Test Time | 88.6% | 88.4% |
| | ATTA Retrained with EF | 91.6% | 91.4% |

Table 5: Square Attack [31] results on 500 samples on settings presented in Table 3. Square Attack does not significantly reduce the robustness of models with *Essential Features*, although some models with Chen et al., such as the Natural Retrained with Chen, experience significant reduction. Our *Essential Features* adaptive attacks perform particularly well on some settings such as the Natural + EF at Test Time settings for RESISC45 and Imagenette, since Square Attack’s robustness is much higher.

| Dataset | Model | Robustness (L_2 Square on 500 Samples) | Robustness (L_∞ Square on 500 Samples) |
|-------------------|-----------------------------|---|--|
| MNIST | Natural | 0.0% | 0.0% |
| | Natural + EF at Test Time | 13.8% | 73.4% |
| | Natural + Chen at Test time | 16.2% | 78.0% |
| | Natural Retrained with EF | 18.6% | 75.2% |
| | Natural Retrained with Chen | 2.4% | 1.6% |
| | ATTA Retrained with Chen | 23.2% | 90.2% |
| Fashion- MNIST | Natural | 10.2% | 7.2% |
| | Natural + EF at Test Time | 14.6% | 21.2% |
| | Natural + Chen at Test time | 9.6% | 42.0% |
| | Natural Retrained with EF | 15.8% | 24.2% |
| | Natural Retrained with Chen | 4.8% | 7.2% |
| | ATTA Retrained with Chen | 20.8% | 69.8% |
| CIFAR-10 | Natural | 39.2% | 0.8% |
| | Natural + EF at Test Time | 19.2% | 2.6% |
| | Natural + Chen at Test time | 32.2% | 0.0% |
| | Natural Retrained with EF | 43.0% | 22.4% |
| | Natural Retrained with Chen | 45.6% | 3.6% |
| | ATTA Retrained with Chen | 45.0% | 50.0% |
| GTSRB | Natural | 42.8% | 35.6% |
| | Natural + EF at Test Time | 44.2% | 46.4% |
| | Natural + Chen at Test time | 50.4% | 42.0% |
| | Natural Retrained with EF | 44.0% | 55.6% |
| | Natural Retrained with Chen | 50.8% | 42.2% |
| | ATTA Retrained with Chen | 67.4% | 78.0% |
| RESISC45 | Natural | 6.2% | 4.8% |
| | Natural + EF at Test Time | 9.2% | 3.0% |
| | Natural + Chen at Test time | 12.4% | 4.2% |
| | Natural Retrained with EF | 28.8% | 12.0% |
| | Natural Retrained with Chen | 9.8% | 4.2% |
| | ATTA Retrained with Chen | 33.6% | 39.6% |
| Imagenette | Natural | 78.8% | 74.4% |
| | Natural + EF at Test Time | 74.4% | 61.2% |
| | Natural + Chen at Test time | 76.4% | 57.4% |
| | Natural Retrained with EF | 88.2% | 81.0% |
| | Natural Retrained with Chen | 84.8% | 66.0% |
| | ATTA Retrained with Chen | 80.6% | 83.0% |

Table 6: Results comparing the full transform with just adaptive blurring and just adaptive color reduction. The full transformation shows clear benefits over just adaptive blurring and helps significantly on CIFAR-10 and RESISC45.

| Dataset | Model | Accuracy | Robustness (L_2 PGD) | Robustness (L_∞ PGD) |
|---------------|-------------------------------|---------------|----------------------------|---------------------------------|
| MNIST | Full EF | 98.43% | 0.00% | 91.00% |
| | Just Adaptive Blur | 96.70% | 0.02% | 84.97% |
| | Just Adaptive Color Reduction | 98.51% | 0.00% | 91.73% |
| Fashion-MNIST | Full EF | 82.06% | 23.37% | 71.54% |
| | Just Adaptive Blur | 81.86% | 20.24% | 69.15% |
| | Just Adaptive Color Reduction | 82.22% | 22.06% | 71.88% |
| CIFAR-10 | Full EF | 84.52% | 38.46% | 51.97% |
| | Just Adaptive Blur | 83.78% | 23.15% | 50.05% |
| | Just Adaptive Color Reduction | 85.27% | 29.45% | 50.14% |
| GTSRB | Full EF | 90.32% | 57.71% | 73.25% |
| | Just Adaptive Blur | 92.15% | 57.17% | 76.32% |
| | Just Adaptive Color Reduction | 91.86% | 58.7% | 76.45% |
| RESISC45 | Full EF | 88.24% | 52.44% | 53.33% |
| | Just Adaptive Blur | 84.07% | 21.47% | 41.38% |
| | Just Adaptive Color Reduction | 83.44% | 30.80% | 45.24% |
| Imagenette | Full EF | 95.34% | 72.28% | 80.71% |
| | Just Adaptive Blur | 94.45% | 66.50% | 76.2% |
| | Just Adaptive Color Reduction | 94.75% | 71.62% | 79.90% |

Table 7: Results comparing the full transform with just adaptive blurring and just adaptive color reduction on Square Attack.

| Dataset | Model | Accuracy | Robustness (L_2 Square on 500 Samples) | Robustness (L_∞ Square on 500 Samples) |
|---------------|-------------------------------|----------|--|---|
| MNIST | Full EF | 98.43% | 16.6% | 89.8% |
| | Just Adaptive Blur | 96.70% | 1.0% | 83.0% |
| | Just Adaptive Color Reduction | 98.51% | 22.0% | 90.2% |
| Fashion-MNIST | Full EF | 82.06% | 50.2% | 68.0% |
| | Just Adaptive Blur | 81.86% | 36.2% | 69.2% |
| | Just Adaptive Color Reduction | 82.22% | 47.0% | 69.4% |
| CIFAR-10 | Full EF | 84.52% | 63.6% | 56.2% |
| | Just Adaptive Blur | 83.78% | 63.2% | 59.0% |
| | Just Adaptive Color Reduction | 85.27% | 64.0% | 65.0% |
| GTSRB | Full EF | 90.32% | 62.0% | 73.8% |
| | Just Adaptive Blur | 92.15% | 59.2% | 77.4% |
| | Just Adaptive Color Reduction | 91.86% | 65.0% | 79.2% |
| RESISC45 | Full EF | 88.24% | 60.8% | 50.6% |
| | Just Adaptive Blur | 84.07% | 52.0% | 64.2% |
| | Just Adaptive Color Reduction | 83.44% | 63.0% | 60.4% |
| Imagenette | Full EF | 95.34% | 91.6% | 91.4% |
| | Just Adaptive Blur | 94.45% | 88.4% | 90.4% |
| | Just Adaptive Color Reduction | 94.75% | 91.4% | 91.0% |